ACS Catalysis

Research Article

pubs.acs.org/acscatalysis

The Strength of Brønsted Acid Sites in Microporous Aluminosilicates

Andrew J. Jones* and Enrique Iglesia*

Department of Chemical and Biomolecular Engineering, University of California, Berkeley, California 94720, United States

Supporting Information

ABSTRACT: Ensemble-averaged deprotonation energies (DPE) derived from periodic density functional theory models are insensitive to the location of isolated Al atoms and associated protons and similar among microporous aluminosilicates (i.e., zeolites) with different crystalline frameworks (MFI, BEA, FER, MOR, CHA, FAU). These DPE values are 1201 ± 11 kJ mol^{-1} after correcting for systematic artifacts of periodic DFT methods, which vary with framework density, and averaging over the four distinct proton locations at each Al atom. These energies rigorously reflect the strength of the acid sites in these important catalytic solids. Thus, the stability of the conjugate anions and the acid strength of these materials merely reflect the presence of Al atoms within the silicate framework, and not their specific siting or local confining environment. DPE values did not show any systematic trends with the vibrational frequency or length of O−H bonds, with Si−O−Al bond angles, or with NH_3 adsorption enthalpies, properties that are frequently but inaccurately used as experimental indicators of acid strength. Such properties may reflect or bring forth confinement effects that do not influence acid strength, but which can stabilize the relevant ion-pair transition states and adsorbed intermediates through dispersion forces. These findings confirm that the different shape and size of the confining voids near Al atoms and their associated protons, instead of any differences in their acid strength, give rise to the remarkable diversity of acid forms of zeolites in the practice of catalysis.

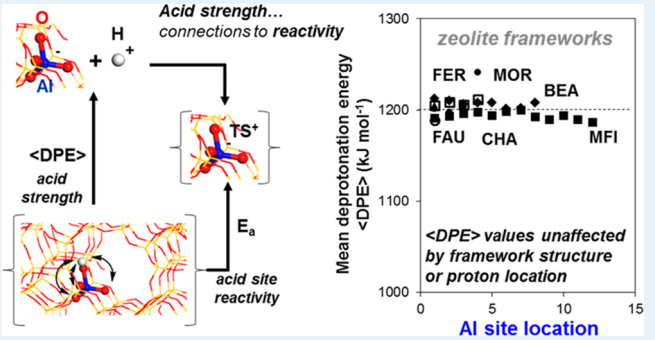

KEYWORDS: *Brønsted acid, deprotonation energy, statistical mechanics, DFT, acid strength*

1. INTRODUCTION

The very diverse reactivity and adsorption properties of microporous aluminosilicates are often ascribed to the effects of the framework structure on the acid strength of their charge-balancing protons. Such different acid strengths have been inferred from the observed effects of zeolite structure on the adsorption enthalpies of probe molecules, such as NH_3 and pyridine.[1−6] Yet, such adsorption enthalpies are not sensitive to the replacement of Al by Fe within H-MFI frameworks, which causes marked changes in turnover rates for methanol dehydration and *n*-hexane cracking.[3,7] Also, van der Waals interactions between molecules and confining zeolite frameworks stabilize adsorbed species and transition states,[8−10] and impart the remarkable catalytic diversity observed for these microporous solid acids.[11] The combined effects of electrostatic interactions, which sense acid strength, and dispersive forces, which reflect the location and properties of protons within aluminosilicate frameworks, account for the stability of the adsorbed intermediates and the ion-pair transition states that determine reactivity and selectivity in acid catalysts.[5,8,9,11,12]

The preeminent effects of van der Waals forces reflect the prevalence of voids of molecular size in these microporous solids; such voids allow effective contacts between guest species and the confining scaffold. These van der Waals forces, however, preclude the accurate determination of acid strength, even on a relative basis, using the binding of probe molecules on protons within different zeolite structures or even at different crystallographic locations within a given framework. Their acid strength, however, can be assessed at each distinct crystallographic location for any zeolite framework using theoretical methods because the crystal structures of such materials are accurately known. The distribution of protons among the distinct crystallographic T-sites present in many zeolite framework is seldom known, but can be inferred in some cases from advanced spectroscopic methods[13−16] or from theoretical and experimental mechanistic analysis of catalytic reactions.[3,5,15]

The strength of a Brønsted acid is rigorously defined by the energy required to separate a proton from its conjugate anion to noninteracting distances. This deprotonation energy (DPE) is given by

$$\mathrm{DPE} = E_{Z^-} + E_{H^+} - E_{ZH} \quad (1)$$

where E_{Z^-}, E_{H^+}, and E_{ZH} are the respective energies of the zeolite anion after deprotonation, of the gaseous proton, and of the neutral H-form of the zeolite. DPE values do not depend on the proton acceptor, thus providing an acid strength scale that is independent of the reacting or adsorbing molecules involved.

Received: June 1, 2015
Revised: August 9, 2015

DOI: 10.1021/acscatal.5b01133
ACS Catal. 2015, 5, 5741−5755

These DPE values cannot be measured, but they can be estimated for zeolites by density functional theory (DFT) using cluster models,[3,17−20] embedding schemes,[21] or periodic structures.[22,23] The reported DPE values for Al-MFI, however, span a very broad range (1205−1414 kJ mol^{-1}) depending on the structural models, functionals, and basis sets used and, in some cases, on the location of the proton and the Al atom. DPE values have been reported for only a small subset of the distinct Si−O(H)−Al locations in MFI zeolites (3 of 48 locations). A rigorous comparison of acid strength among different frameworks requires accurate DPE values at each accessible location in a given structure, as well as the rigorous averaging of these DPE values among such locations using statistical mechanics methods that account for the mobility and distribution of protons among the O atoms at each Al location at the temperatures relevant to catalysis.

We report here DPE values at each distinct Si−O(H)−Al crystallographic location in MFI, BEA, MOR, FER, CHA, and FAU zeolite frameworks using periodic DFT methods that avoid the termination and embedding artifacts ubiquitous in cluster models,[23] and which allow for the systematic change in proton and Al location without affecting the size and shape of the zeolite model. We show that while DPE values can differ among Al and H$^+$ locations, the average acid strength of their statistical ensembles (at each Al atom) differs negligibly among Al locations. Ensemble-averaged DPE values accurately reflect the acid strength values that determine measured catalytic reactivity, because the relevant transition states reflect analogous ensemble averaging at each Al atom location.

We also assess in this study the consequences of the location of Al and O atoms, of the Si−O−Al bond angles, and of the frequency of O−H stretches (ν(OH)) on DPE values in order to probe any plausible relations between the local framework structure and the strength of the associated Brønsted acid sites. Finally, we provide evidence that while NH_3 adsorption energies depend sensitively on the location of the H$^+$ and of the NH_4^+ cations formed, they do not sense the differences in acid strength that are actually relevant for catalytic reactivity because of the combined attenuation of acid strength differences to the formation energy of NH_4^+ cations and the marked effects of dispersive interactions, unrelated to acid strength, between NH_4^+ and the confining voids on adsorption energies.

2. METHODS

2.1. Density Functional Theory Calculations of Deprotonation Energy and ν(OH) Frequencies. DPE values were calculated from geometry optimizations of neutral (ZH) and deprotonated (Z$^-$) periodic zeolite structures of MFI, BEA, FER, MOR, CHA, and FAU frameworks using plane-wave periodic gradient-corrected DFT methods, as implemented in the Vienna ab initio Simulation Package (VASP),[24−27] using a plane-wave energy cutoff of 396 eV, Revised Perdew−Burke−Ernzerhof (RPBE) functional,[28] and a plane-wave basis set of the projector-augmented-wave (PAW) method.[29,30] All atoms were relaxed until electronic energies varied by < 1×10^{-6} eV, and the forces on all atoms were < 0.01 eV Å^{-1}. A $(1 \times 1 \times 1)$ γ-centered k-point mesh was used to sample the first Brillouin zone for all zeolite cells. DPE values are reported as the energy required in order to cleave the H atoms heterolytically from the zeolite framework to form a H$^+$ and a zeolite anion (Z$^-$), eq 1. Here, E_{Z^-}, E_{H^+}, and E_{ZH} are the electronic energies of the deprotonated zeolite anion, a bare proton, and the neutral Brønsted acid, respectively. Free energies were estimated from the sum of electronic energies, zero-point vibrational energies, and thermal contributions to energy and entropies determined from vibrational frequency calculations at 433 K. The vibrational frequencies of O−H bonds were obtained from the Hessian matrix using the harmonic approximation.[31]

The atomic coordinates and unit cell parameters of BEA (a = b = 1.2632, c = 2.6186 nm and $\alpha = \beta = \gamma = 90°$), FER ($a$ = 1.9018, b = 1.4303, c = 0.7541 nm and $\alpha = \beta = \gamma = 90°$), MOR ($a$ = 1.8256, b = 2.0534, c = 0.7542 nm and $\alpha = \beta = \gamma = 90°$), CHA ($a = b$ = 1.3675, c = 1.4767 nm and $\alpha = 90°$, $\beta = 90°$, $\gamma = 120°$), and FAU ($a = b = c$ = 2.4345 nm and $\alpha = \beta = \gamma = 90°$) were taken from the International Zeolite Association (IZA) Web site.[32] Orthorhombic MFI structures (a = 2.0022, b = 1.9899, c = 1.3383 nm and $\alpha = \beta = \gamma = 90°$) were determined from X-ray diffractograms (0.32 Al/u.c.).[33] The numbering convention of Olson et al.[34] is used throughout for MFI structures; other structures follow the numbering convention defined in their respective IZA crystallographic information files.[32] Supercells composed of two unit cells along the c lattice vector $(1 \times 1 \times 2)$ were constructed and used for FER (i.e., 1.9018 × 1.4303 × 1.5082 nm^3) and MOR (i.e., 1.8256 × 2.0534 × 1.5084 nm^3) to minimize interactions between periodic unit cells by maintaining > 1.2 nm spatial separations of atoms from their periodic images for all zeolites. Lattice constants and angles were used without relaxation for all zeolites.

Charged defects, such as those created after the deprotonation of a zeolite, in periodic calculations can introduce artificial interactions among defects in neighboring cells. These interactions are mitigated in VASP by the introduction of a neutralizing background charge, but such treatments require large supercells to minimize spurious interactions and often do not lead to the correct defect energies.[35,36] A posteriori corrections to defect formation energies[35] increased the DPE values of MFI and BEA (by 71 and 53 kJ mol^{-1}, respectively) instead of bringing them closer to expected DPE values (these artifacts of periodic DFT are discussed further in section 3.3). These results indicate that more accurate treatments of charged cells are required for accurate defect formation energies of periodic systems. Defect formation energy artifacts within a given periodic structure, however, are insensitive to the location of the Al or proton because of the localized nature of the framework negative charge and the large size of the super cells;[3] for example, DPE differences in FER among seven H$^+$ and Al configurations were within 8 kJ mol^{-1} when calculated with periodic DFT (PBE functionals) or embedded-cluster (PBE functionals) methods.[23] Therefore, DPE values are compared within a given zeolite framework without further correcting these periodic interactions. DPE comparisons among zeolite frameworks are discussed in section 3.3.

2.2. DFT Calculations of NH_3 Adsorption Energies. The adsorption energies of NH_3 on Brønsted acid sites in zeolites were determined from the geometry-optimized structures of the NH_4^+-form and the H$^+$-form zeolites,

$$E_{NH_3(ads)} = E_{NH_4^+Z^-} - E_{ZH} - E_{NH_3} \quad (2)$$

where $E_{NH_4^+Z^-}$, E_{ZH}, and E_{NH_3} are the electronic energies of the NH_4^+-form zeolite, the bare zeolite, and $NH_{3(g)}$, respectively. MFI structures were optimized using the protocols outlined in section 2.1, except that the PBE-D2 functional of Grimme[37]

DOI: 10.1021/acscatal.5b01133
ACS Catal. 2015, 5, 5741−5755

was used to properly account for dispersive interactions of NH_4^+ with the zeolite framework (instead of the RPBE functional). The accessibility of NH_3 molecules to specific protons was determined with the Zeo++[38,39] program using previously described protocols.[5] Frequency calculations on optimized structures were used to determine zero-point vibrational energies and temperature-dependent vibrational energy corrections to the enthalpies and free energies at 480 K, a temperature chosen to illustrate their values at conditions typical of catalysis.

2.3. Statistical Treatments of Energies for Equilibrated Systems. The proton that balances the charge at each Al heteroatom in a siliceous zeolite framework can occupy locations centered atop each of the four O atoms that are bound to each Al atom (Scheme 1). These four distinct

Scheme 1. Schematic of Zeolite Proton Energies and Deprotonation Energies As a Function of Proton Location at a Given Al T-site and the Energy of the Ensemble-Averaged Structure

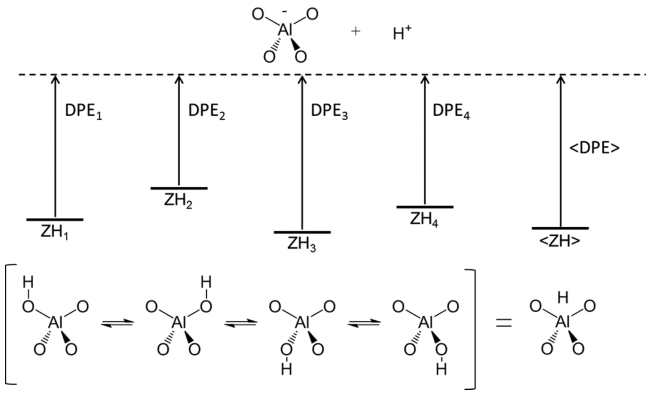

locations represent local energy minima characterized by different DPE values, which reflect their respective O−H bond energies relative to a proton at a noninteracting distance and a common conjugate anion that exhibits the same energy and electronic structure irrespective of the original location from which the proton was removed. The infrared spectra of pyridine adsorbed on FAU show that proton migration among all four O atoms at an Al site is fast, even at ambient temperatures.[40] Such facile hopping is consistent with DFT treatments and with the ubiquitous presence of H_2O, which mediates proton hopping, even in catalytic amounts.[41]

The energy of a Brønsted acid site at any given time depends on the location of the proton at that time. When the occupancies of the four proton locations are set by thermodynamic equilibrium, the energy (expected value) is given by the sum of the energies of each of the four states each multiplied by the probability that the proton is in that state. The (expected) energy value of this equilibrated system ($\langle E_{ZH}\rangle$) is given by its Boltzmann average over the energies ($E_{ZH,i}$) and free energies ($G_{ZH,i}$) of each of these four states

$$\langle E_{ZH}\rangle = \frac{\sum_{i=1}^{4}\left[E_{ZH,i}\exp\left(\frac{-G_{ZH,i}}{k_BT}\right)\right]}{\sum_{i=1}^{4}\exp\left(\frac{-G_{ZH,i}}{k_BT}\right)} \quad (3)$$

This expected energy ($\langle E_{ZH}\rangle$) will be denoted here as the ensemble-averaged energy. The strength of a Brønsted acid site under the conditions of its use in catalysis thus depends on the Al location and the distribution of protons at a given temperature. This is reflected in DPE values calculated with respect to the ensemble-averaged energy of these protons

$$\langle \mathrm{DPE}\rangle = E_{Z^-} + E_{H^+} - \langle E_{ZH}\rangle \quad (4)$$

where $\langle$DPE$\rangle$ is the ensemble-averaged DPE value under conditions that allow equilibration of protons among the four possible locations at each Al location.

3. RESULTS AND DISCUSSION

3.1. DPE of Zeolites from Density Functional Theory Treatments. DFT-derived DPE values are shown in Figure 1 and Table 1 for each distinct Al and H^+ location in MFI, BEA, FER, MOR, CHA, and FAU zeolites using crystal structures containing one proton per unit cell (or super cell in the case of FER and MOR; section 2.1). DPE values differ by up to 77 kJ mol^{-1} (<47, <31, < 8, <77, <7, <6 kJ mol^{-1} for MFI, BEA, FER, MOR, CHA, and FAU) among all O-atom and Al-atom locations for each zeolite framework (Figure 1). This range of DPE values reflects the different stability of the protons bound to O atoms at each different Al location, but also that of the protons at each of the crystallographically unique O atoms for each Al location. The even larger DPE differences among zeolite frameworks (up to 164 kJ mol^{-1}) reflect an artifact of periodic DFT methods as implemented in VASP, as discussed in section 3.3.

The substitution of a Si atom by an Al atom at the T8 location in MFI (notation by convention[34]) is accompanied by a charge-balancing proton that can reside at any of the four O atoms (O12, O13, O7, O8) to which the Al is connected. The DPE values differ by 36 kJ mol^{-1} among these locations (between Al8−O7(H)−Si7 and Al8−O12(H)−Si12). Also, the proton at the O12 atom may charge-balance an Al atom at either the T8 or the T12 Al position. The DPE value of the proton at the O12 atom is 24 kJ mol^{-1} larger when the Al is at the T12 (Al12−O12(H)-Si8) instead of the T8 (Al8−O12(H)−Si12) position. Such a dependence of DPE on the location of a proton among vicinal O atoms and on Al siting within MFI frameworks was also evident for other frameworks (BEA, MOR, FAU, CHA, FER; Figure 1). Thus, we conclude that these DPE values sense subtle differences in the location of *both* the protons *and* the Al atoms within the void space where catalytic reactions occur. The unsettling nature of these effects of location on DPE for structures with similar composition is resolved later in this work and shown to have negligible consequences on acid catalysis, when DPE values are appropriately averaged among such locations; in such averaging, we account for the mobility and distribution of protons and for how chemical reactions statistically average the relevant ion-pair transition energies among such locations at temperatures relevant for catalysis.

The magnitude of the DPE values derived from periodic DFT and QM-Pot[21] DFT methods differ significantly (e.g., 1668 and 1200 kJ mol^{-1}, respectively, for Al7−O17(H)−Si4 in MFI). The larger DPE values derived from periodic DFT methods reflect artifacts introduced by the periodic interactions of charged structures (section 2.1),[35,36,42] but also the ill-defined nature of charge within a periodic cell, as discussed in more detail in section 3.3. DPE values from periodic DFT models differ among the different frameworks (by up to 164 kJ mol^{-1}; Figure 1), at least in part because of their different framework densities (section 3.3). These ubiquitous artifacts influence DPE values at all locations in a given framework,

DOI: 10.1021/acscatal.5b01133
ACS Catal. 2015, 5, 5741−5755

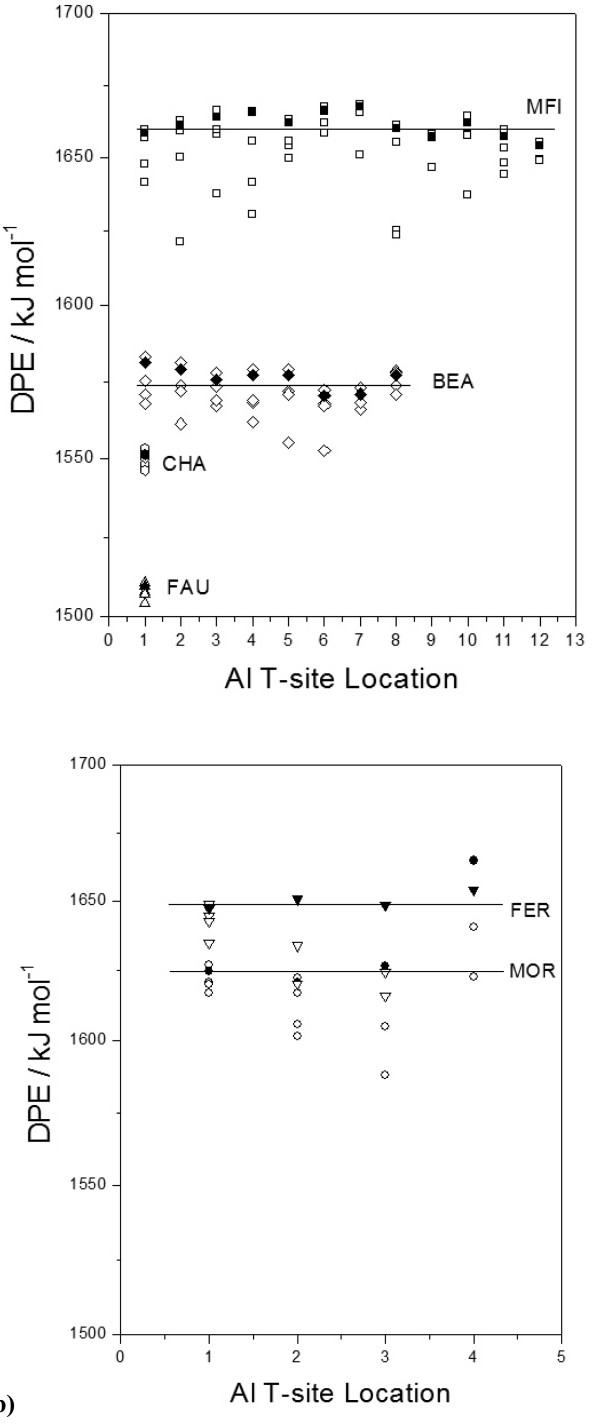

Figure 1. DPE values of zeolites with Al and H^+ at all crystallographically unique configurations (open symbols) in (a) MFI (squares), BEA (diamonds), FAU (triangles), and CHA (hexagon) and (b) FER (upside-down triangle) and MOR (circles) calculated with periodic DFT at the RPBE/PAW level. Ensemble-averaged DPE values at 433 K calculated with eqs 3 and 4 are included as closed symbols for each Al site configuration.

however, to the same extent, thus allowing DPE values to be compared accurately within a given framework structure.

3.2. The Influence of Zeolite Structure on DPE Values.

Any effects of proton and Al locations on DPE must reflect local differences in framework structure, because the negative charge that forms upon deprotonation remains within the second-coordination sphere O atoms from the Al.[3,17,18] Figure 2 shows Si−O−Al bond angles of Si−O(H)−Al bridging structures and their DPE values as a function of their assigned configuration number (given in Table 1; in ascending order of DPE values) for MFI, BEA, FER, MOR, CHA, and FAU. These Si−O−Al bond angles (126−148°) differ among Al and H^+ locations, with smaller bond angles frequently, but not always, associated with larger DPE values (Figure 2); the fact that larger DPE values do not, in general, tend to correspond to smaller bond angles negates any meaningful correlation between the two properties, as also concluded[43] from DPE values calculated at the four proton locations at the unique Al site in FAU and for three configurations (three different Al sites with a single proton location at each) in MFI using QM-Pot DFT methods.

These weak and uncorrelated effects of bond angles on DPE values and on the stability of Si−O(H)−Al structures indicate that such bond angles do not directly influence acid strength. This conclusion is consistent with the numerous configurations with different bond angles but similar DPE values (e.g., configurations 17 and 18 of MFI have equivalent DPE values of 1651 kJ mol^{-1}, but bond angles of 135° and 130°, respectively; Table 1). These weak or nonmonotonic effects of bond angles on DPE may also reflect, in some cases, the similar consequences of such bond angles for protonated (neutral) and deprotonated (anionic) structures; for instance, the larger Si−O−Al bond angle in configuration 6 relative to configuration 5 (144° vs 137°) leads to a H-form zeolite structure that is less stable (by 6 kJ mol^{-1}; E_{ZH} in eq 1) than the latter and to a deprotonated structure that is also less stable (also by 6 kJ mol^{-1}; E_{Z^-} in eq 1) than the latter, thus attenuating any consequences of bond angles on DPE values (to < 1 kJ mol^{-1}) and acid strength. These results indicate that DPE differences among zeolites, if they exist, could not be inferred from or caused by their different Si−O−Al bond angles.

Figure 3a shows ν(OH) stretching frequencies (2910−3630 cm^{-1}) for each proton and Al location together with the respective DPE values for MFI, BEA, FER, MOR, CHA, and FAU frameworks. These ν(OH) values tend to parallel DPE values (c.f., Figure S.1, Supporting Information), but with many large deviations predominantly corresponding to locations with ν(OH) frequencies well below the trends observed for other locations, as shown previously for paired and isolated sites in FER.[23] The ν(OH) values for each proton location correlate well with O−H bond distances for all zeolite frameworks (Figure 3b); this well-known inverse relation between frequency and small variations in bond distance is commonly known as Badger's rule, which relates the force constant for stretching a bond to the equilibrium bond length.[44] O−H bond distances are similar (80% are 0.96−0.98 Å) to the average O−H bond distances measured by NMR (0.96−0.98 Å) on MFI samples at 183 K.[45,46] The statistically averaged O−H bond distance of MFI at 183 K (calculated from eq 3 applied to the four protons around each Al with bond distances replacing the proton energy ($E_{ZH,i}$) and the arithmetic mean of the resulting expected bond distances over all T-sites), assuming all T-sites have an equal probability of having an Al, is 0.98 ± 0.01 Å, consistent with the spectroscopic observations of NMR on MFI samples at 183 K with unknown Al siting.

O−H bonds are typically longer within more confining locations (Figure 4); the extent of confinement is approximated from the attractive portions of Lennard-Jones potentials between the proton and the zeolite framework,

DOI: 10.1021/acscatal.5b01133
ACS Catal. 2015, 5, 5741−5755

Table 1. DPE, ν(OH) Frequency, Si−O−Al Bond Angle, and O−H Bond Distances (d(O−H)) for Each Distinct Al and H^+ (shown as O number) Location in (a) MFI, (b) BEA, (c) FER, (d) MOR, (e) CHA, and (f) FAU Frameworks

(a) MFI (12 T-sites)

configuration	T-site substitution	H^+ binding location	DPE/kJ mol^{-1}	ν(OH)/cm^{-1}	Si−O−Al angle/deg	d(O−H)/Å
1	Al2	O13	1621	3551	141.1	0.979
2	Al8	O13	1624	3517	142.6	0.980
3	Al8	O12	1625	3339	136.8	0.989
4	Al4	O3	1631	3524	143.8	0.980
5	Al10	O9	1637	3574	136.7	0.977
6	Al3	O3	1638	3521	144.2	0.980
7	Al4	O16	1642	3451	140.6	0.983
8	Al1	O16	1642	3462	141.0	0.982
9	Al11	O14	1644	3298	140.7	0.991
10	Al9	O9	1647	3160	136.2	0.997
11	Al1	O1	1648	3597	134.0	0.977
12	Al11	O22	1648	3613	129.0	0.976
13	Al12	O24	1649	3569	141.5	0.979
14	Al12	O12	1649	3252	139.7	0.993
15	Al5	O14	1650	3472	141.6	0.983
16	Al2	O1	1650	3556	136.1	0.979
17	Al7	O23	1651	3569	135.0	0.979
18	Al7	O22	1651	3620	130.4	0.975
19	Al11	O11	1653	3618	130.3	0.975
20	Al12	O20	1654	3607	134.8	0.976
21	Al5	O21	1654	3605	133.5	0.976
22	Al8	O8	1655	3432	135.9	0.985
23	Al12	O11	1655	3633	129.9	0.974
24	Al4	O4	1656	3553	135.7	0.980
25	Al5	O4	1656	3537	136.3	0.980
26	Al1	O21	1657	3624	132.2	0.975
27	Al9	O18	1657	3608	132.9	0.976
28	Al9	O25	1657	3601	134.8	0.976
29	Al10	O26	1658	3613	131.8	0.976
30	Al3	O2	1658	3615	132.9	0.975
31	Al9	O8	1658	3373	134.1	0.987
32	Al10	O15	1658	3608	128.7	0.976
33	Al6	O18	1659	3605	135.2	0.976
34	Al2	O2	1659	3616	132.1	0.975
35	Al11	O10	1660	3222	139.1	0.995
36	Al1	O15	1660	3586	130.1	0.977
37	Al3	O20	1660	3613	130.8	0.975
38	Al8	O7	1661	3187	135.6	0.996
39	Al6	O19	1662	3253	135.2	0.993
40	Al2	O6	1663	3025	133.0	1.003
41	Al5	O5	1663	3632	127.4	0.974
42	Al10	O10	1664	3158	137.3	0.998
43	Al7	O7	1666	3093	134.7	1.001
44	Al4	O17	1666	3609	130.4	0.976
45	Al6	O6	1666	3462	130.8	0.982
46	Al3	O19	1666	3132	135.5	0.999
47	Al6	O5	1667	3616	125.8	0.975
48	Al7	O17	1668	3627	129.1	0.975

(b) BEA (8 T-sites)

configuration	T-site substitution	H^+ binding location	DPE/kJ mol^{-1}	ν(OH)/cm^{-1}	Si−O−Al angle/deg	d(O−H)/Å
1	Al6	O14	1553	2910	146.1	1.009
2	Al5	O14	1555	2941	144.8	1.007
3	Al2	O4	1561	3497	138.9	0.981
4	Al4	O9	1562	3516	140.7	0.981
5	Al7	O17	1566	3616	134.2	0.976
6	Al3	O8	1567	3618	130.9	0.975
7	Al6	O17	1567	3581	135.0	0.978
8	Al6	O12	1568	3448	131.0	0.984

DOI: 10.1021/acscatal.5b01133
ACS Catal. 2015, 5, 5741−5755

Table 1. continued

(b) BEA (8 T-sites)						
configuration	T-site substitution	H^+ binding location	DPE/kJ mol^{-1}	ν(OH)/cm^{-1}	Si−O−Al angle/deg	d(O−H)/Å
9	Al1	O4	1568	3547	137.3	0.979
10	Al7	O7	1568	3601	134.3	0.977
11	Al4	O11	1568	3610	132.3	0.976
12	Al3	O9	1569	3561	139.2	0.978
13	Al4	O5	1569	3608	131.8	0.976
14	Al9	O15	1571	3595	135.0	0.977
15	Al7	O8	1571	3621	130.1	0.975
16	Al1	O3	1571	3626	129.8	0.975
17	Al5	O15	1571	3325	140.6	0.990
18	Al5	O10	1572	3568	131.5	0.978
19	Al2	O7	1572	3601	135.1	0.976
20	Al6	O16	1572	3247	134.7	0.994
21	Al7	O13	1573	3481	134.1	0.982
22	Al3	O1	1574	3609	130.8	0.976
23	Al8	O11	1574	3601	129.7	0.977
24	Al2	O5	1574	3605	131.6	0.976
25	Al1	O1	1575	3604	131.4	0.976
26	Al9	O3	1578	3608	131.4	0.976
27	Al3	O10	1578	3272	132.1	0.993
28	Al8	O16	1578	3308	134.4	0.990
29	Al5	O13	1579	3300	133.6	0.991
30	Al4	O12	1579	3204	131.0	0.996
31	Al2	O6	1581	3069	130.9	1.002
32	Al1	O2	1583	3090	131.4	1.001
(c) FER (4 T-sites)						
configuration	T-site substitution	H^+ binding location	DPE/kJ mol^{-1}	ν(OH)/cm^{-1}	Si−O−Al angle/deg	d(O−H)/Å
1	Al3	O8	1616	3596	138.9	0.977
2	Al3	O8	1616	3596	138.9	0.977
3	Al2	O5	1620	3552	129.6	0.978
4	Al3	O7	1625	3610	133.1	0.976
5	Al2	O6	1634	3563	143.8	0.979
6	Al2	O6	1634	3563	143.8	0.979
7	Al1	O4	1635	2968	144.0	1.007
8	Al1	O3	1643	3607	134.9	0.976
9	Al1	O1	1645	3618	133.4	0.975
10	Al3	O1	1648	3605	132.4	0.976
11	Al1	O2	1649	3592	130.1	0.976
12	Al2	O2	1651	3599	130.8	0.976
13	Al4	O7	1654	3618	133.0	0.975
14	Al4	O7	1654	3618	133.0	0.975
15	Al4	O5	1654	3446	130.6	0.984
16	Al4	O5	1654	3446	130.6	0.984
(d) MOR (4 T-sites)						
configuration	T-site substitution	H^+ binding location	DPE/kJ mol^{-1}	ν(OH)/cm^{-1}	Si−O−Al angle/deg	d(O−H)/Å
1	Al3	O8	1588	3594	136.3	0.977
2	Al2	O7	1602	3608	132.3	0.976
3	Al3	O9	1605	3200	144.9	0.995
4	Al2	O6	1606	3521	147.6	0.981
5	Al1	O3	1617	3575	141.3	0.978
6	Al2	O5	1617	3609	134.7	0.976
7	Al1	O2	1620	3598	137.5	0.977
8	Al1	O1	1621	3604	135.3	0.976
9	Al2	O4	1622	3601	137.2	0.977
10	Al4	O10	1623	3613	135.6	0.976
11	Al3	O3	1627	3618	128.1	0.975
12	Al3	O3	1627	3618	128.1	0.975
13	Al1	O4	1627	3591	134.4	0.977
14	Al4	O9	1641	2998	141.9	1.004
15	Al4	O7	1665	3613	130.6	0.975

DOI: 10.1021/acscatal.5b01133
ACS Catal. 2015, 5, 5741−5755

Table 1. continued

(d) MOR (4 T-sites)						
configuration	T-site substitution	H^+ binding location	DPE/kJ mol^{-1}	ν(OH)/cm^{-1}	Si−O−Al angle/deg	d(O−H)/Å
16	Al4	O7	1665	3613	130.6	0.975
(e) CHA (1 T-site)						
configuration	T-site substitution	H^+ binding location	DPE/kJ mol^{-1}	ν(OH)/cm^{-1}	Si−O−Al angle/deg	d(O−H)/Å
1	Al1	O2	1546	3593	134.4	0.977
2	Al1	O1	1548	3606	132.2	0.976
3	Al1	O3	1550	3597	135.1	0.977
4	Al1	O4	1553	3615	131.3	0.975
(f) FAU (1 T-site)						
configuration	T-site substitution	H^+ binding location	DPE/kJ mol^{-1}	ν(OH)/cm^{-1}	Si−O−Al angle/deg	d(O−H)/Å
1	Al1	O3	1504	3543	130.7	0.979
2	Al1	O4	1507	3617	129.8	0.975
3	Al1	O2	1508	3571	127.9	0.977
4	Al1	O1	1511	3624	127.6	0.975

$$\eta_{conf} \equiv \sum_i r_i^{-6} \quad (5)$$

where r_i is the distance between the proton and a zeolite O atom (not including the O atom bound to the proton). Tighter voids, with concomitantly more intimate contact between protons and zeolite framework O atoms, lead to larger proton confinement factors, η_{conf}. The excellent correlation between these proton confinement factors and O−H bond lengths (Figure 4), and thus also with ν(OH) frequencies (Figure 3b), indicates that any observed differences in ν(OH) values reflect the different confinement of protons, instead of any differences in their acid strength. In effect, proton locations that exhibit more intimate proton-framework contacts and more effective dipole−dipole (and dispersive) interactions lead to longer O−H bonds and smaller ν(OH). Thus, ν(OH) values (and the O−H distances with which they correlate) are inappropriate proxies for acid strength, a property of the solid acid that predominantly reflects the stability of the conjugate anion, and not the strength of the weak long-range interactions between protons and zeolite frameworks. The confinement of protons does not appreciably influence DPE values, in spite of the presence of these interactions in DPE, because of the negligible differences in energy of these interactions when compared with the electrostatic energy required to remove the proton completely.

We conclude that Si−O−Al bond angles, O−H bond distances, and ν(OH) frequencies cannot accurately describe any framework properties directly related to acid strength, as defined by DPE values. We do not find any evidence to support the proposed use of these structural or spectral features as descriptors of the strength of Brønsted acid sites present within microporous aluminosilicate frameworks.

3.3. Statistical Mechanics Treatments of DPE Ensemble Averages. The ensemble-averaged ⟨DPE⟩ values (from eqs 3 and 4; section 2.3) are shown in Figure 1 at 433 K (a temperature chosen as an illustrative example of a typical value for CH_3OH dehydration[47] in zeolites) for each of the 12, 8, 4, 4, 1, and 1 distinct Al sites in MFI, BEA, MOR, FER, CHA, and FAU, respectively. On each sample with multiple Al T sites, these ⟨DPE⟩ values varied only very slightly with Al location (±7, 5, 22, 3 kJ mol^{-1} for MFI, BEA, MOR, FER; FAU and CHA have only one unique Al). These differences lie within the errors of DFT methods and the inaccuracies of zeolite structural models (except for the values for MOR, as discussed below), indicating that the acid strengths of Brønsted acid sites are insensitive to Al location for any isolated Al atom present within a given zeolite framework. These conclusions are valid only for isolated Al sites; the presence of Al-atom next-nearest-neighbor pairs (Al−O−Si−O−Al) can and does lead to higher DPE values for the associated protons on H-FER (by about 37 kJ mol^{-1}).[23] The exponential averaging of ⟨DPE⟩, in effect, erases the differences observed in DPE values for protons at each of the four O atoms because more stable protons contribute more to the ensemble distributions of protons in equilibrium at each given Al location, making ensemble-averaged DPE values essentially independent of Al location (Scheme 1). These conclusions also hold for ⟨DPE⟩ values calculated at temperatures lower and higher than 433 K; from 100 to 1000 K, each ⟨DPE⟩ value decreases by a similar 3 kJ mol^{-1}, thus keeping the ⟨DPE⟩ range and the conclusions unchanged.

The similar ⟨DPE⟩ values among the 12 distinct Al T-sites in MFI (±7 kJ mol^{-1}) indicate that the intrinsic acid strength of protons does not depend on the Al framework location; instead, acid strength depends only on the identity of the heteroatom (e.g., Al, Ga, Fe, B).[3] The insulating nature of aluminosilicate frameworks,[3,17] taken together with these similar ensemble-averaged ⟨DPE⟩ values at distinct Al T-sites in diverse MFI, BEA, MOR, FER, CHA, and FAU frameworks, indicate that zeolite frameworks, which share similar local structural features and aluminosilicate compositions with the ones examined here, would in general also exhibit similar acid strengths.

We note, however, that ⟨DPE⟩ values differ by as much as 155 kJ mol^{-1} among zeolites with different frameworks and unit cell size, even at locations that share similar local structural features among these frameworks; in the case of MFI, these values are ∼400 kJ mol^{-1} larger than those derived from DFT methods using cluster models[3] or QM-Pot methods.[21,43] These large ⟨DPE⟩ differences are likely to reflect artifacts in DFT treatments of charged periodic unit cells as implemented in VASP (section 2.1), resulting from spurious interactions of these charges among neighboring cells at their periodic boundaries[23,35,36] or from arbitrary energy references used for non-neutral structures in periodic calculations. It is not possible to rigorously remove the interactions of periodic charge interactions because dipole and quadrupole moments cannot be calculated from a unit cell within which some atoms lie very

DOI: 10.1021/acscatal.5b01133
ACS Catal. 2015, 5, 5741−5755

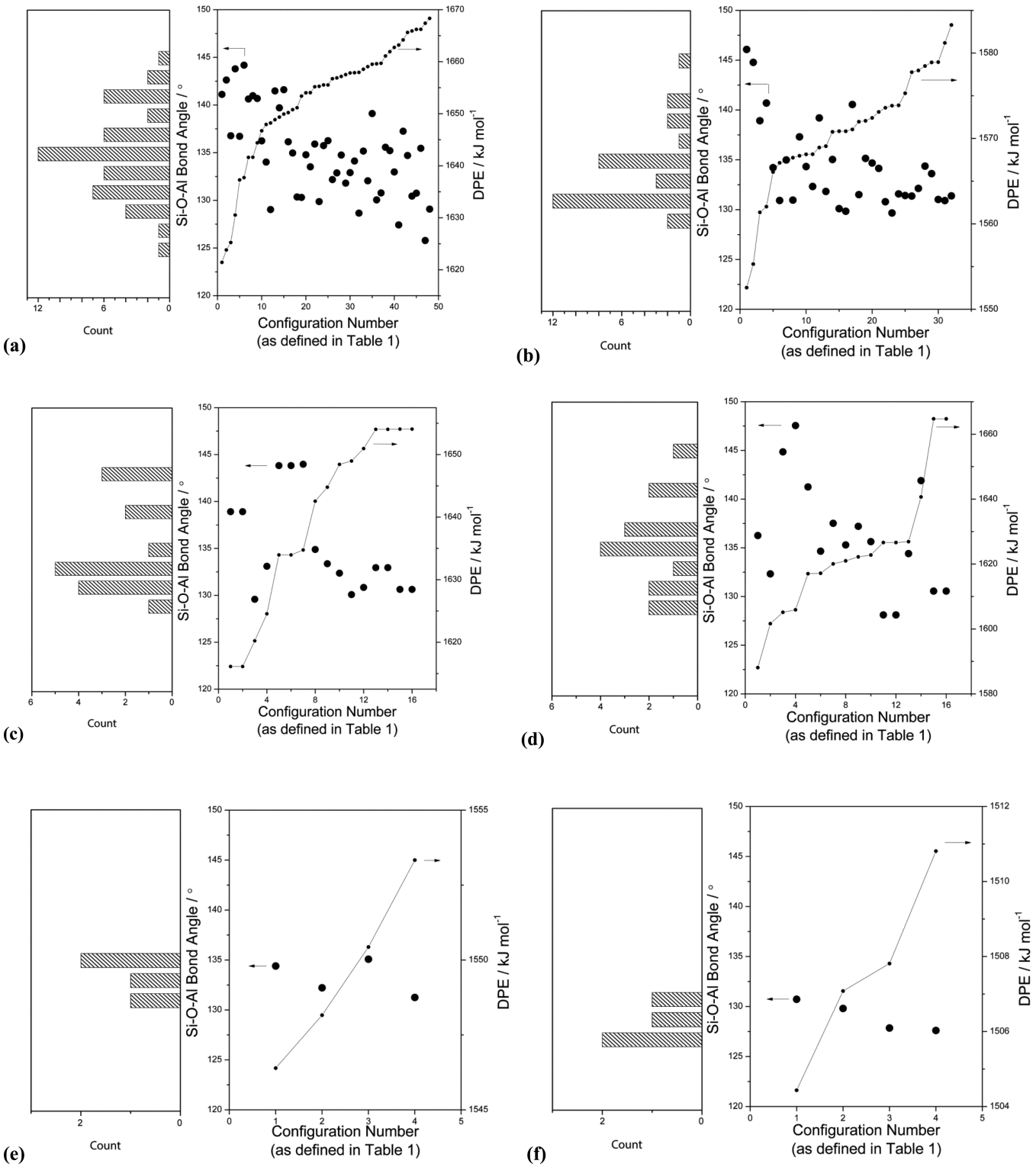

Figure 2. Si−O−Al bond angles and DPE values of Al and H^+ configurations in (a) MFI, (b) BEA, (c) FER, (d) MOR, (e) CHA, and (f) FAU frameworks calculated with periodic DFT at the RPBE/PAW level. Configurations as indicated in Table 1. Histograms display bond angle distributions.

close to the unit cell boundary. Approximate a posteriori treatments have been proposed,[35,42] but their application to MFI and BEA zeolites actually increased DPE values (by 71 and 53 kJ mol^{-1}, respectively), thus making them even more different from those derived from cluster and QM-Pot models; thus, we conclude that these large deviations (~400 kJ mol^{-1}) do not arise from the interactions between periodic cells that these methods intend to correct. These errors must reflect to some extent a systematic ill-defined reference energy in periodic systems with charged unit cells, but the exact cause is not yet known.

DOI: 10.1021/acscatal.5b01133
ACS Catal. 2015, 5, 5741−5755

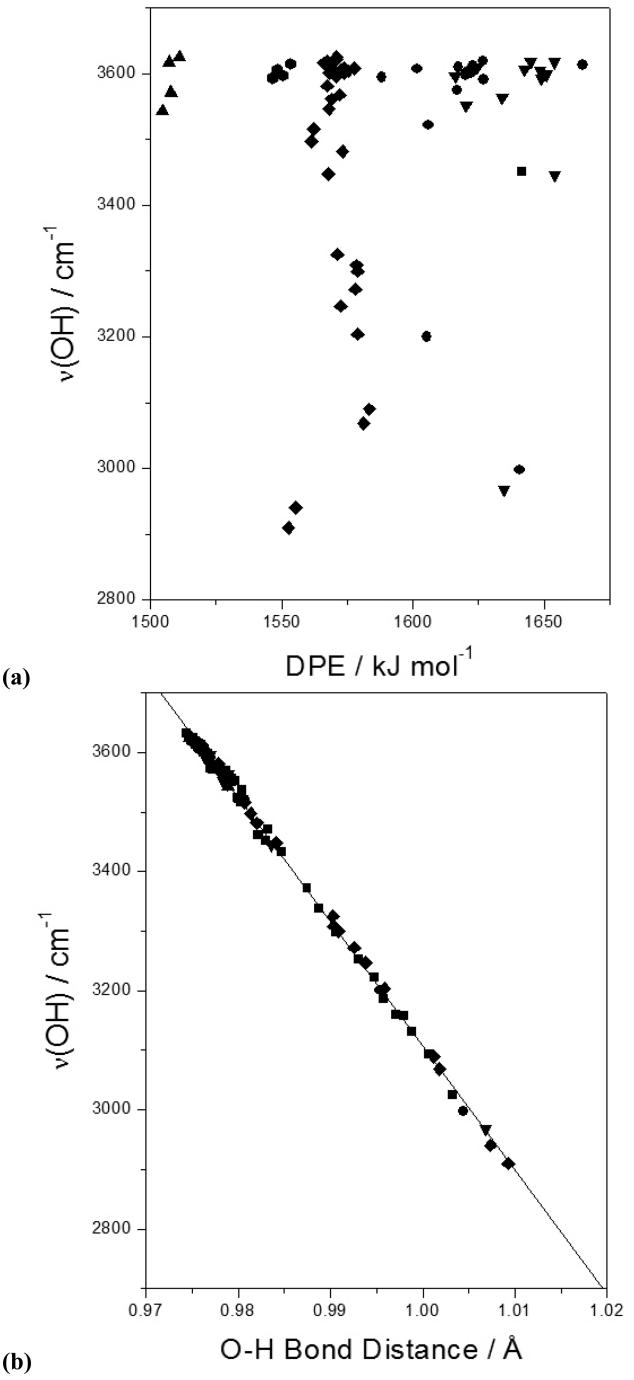

Figure 3. ν(OH) stretching frequencies as a function of (a) DPE and (b) O−H bond distances at various Al and H^+ configurations in MFI (squares), BEA (diamonds), FAU (triangles), CHA (hexagon), FER (upside-down triangle), and MOR (circles) frameworks calculated with periodic DFT at the RPBE/PAW level. Line in b is regressed fit of data for all zeolites.

The periodic DFT artifacts that result in DPE values ~400 kJ mol^{-1} larger than those from other DFT methods preclude any rigorous DPE comparisons among zeolite frameworks. Yet, these artifacts depend, at least in part, on the density of electrons in a given calculation cell that screens the interactions between periodic cells; Figure 5 shows that the arithmetic mean of ⟨DPE⟩ ($\overline{\langle DPE \rangle}$) among all Al configurations in each MFI, BEA, MOR, FER, CHA, and FAU are proportional to their respective framework densities (T atoms per unit cell volume;

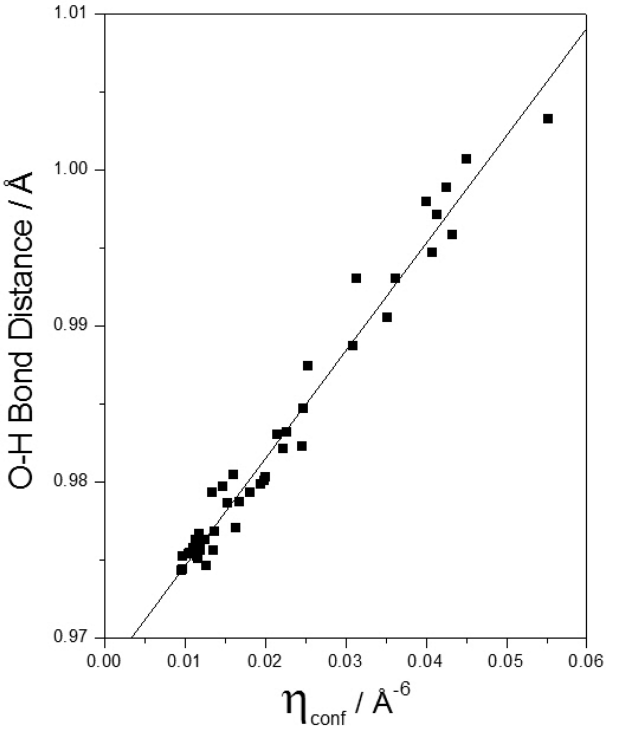

Figure 4. Brønsted O−H bond distances as a function of proton confinement, η_{conf}, eq 5, at various Al and H^+ configurations in MFI calculated with periodic DFT (RPBE/PAW). The line is the regressed fit of the data.

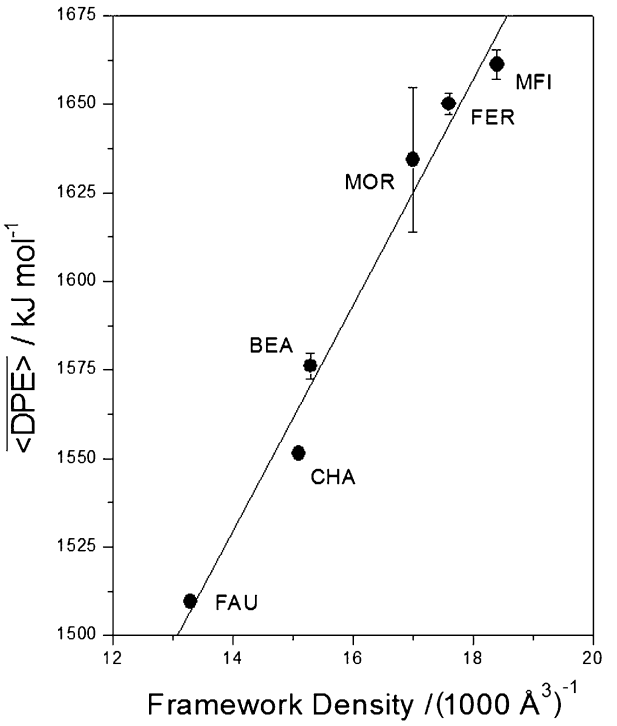

Figure 5. Arithmetic mean of ⟨DPE⟩ values ($\overline{\langle DPE \rangle}$) of zeolites at all Al configurations calculated with eqs 3 and 4 with energies and free energies from DFT (RPBE/PAW) as a function of the framework density[32] (T atoms per volume). The solid line is the regressed fit of the data, and error bars are standard deviations from the mean.

DOI: 10.1021/acscatal.5b01133
ACS Catal. 2015, 5, 5741−5755

from IZA[32]). The arithmetic mean is more appropriate than the exponential mean for averaging ⟨DPE⟩ for the purposes of comparing errors in periodic DFT because these errors depend on the framework density rather than free energy differences in structures. Figure 5 implies that the primary differences in ⟨DPE⟩ between zeolite frameworks do not reflect concomitant differences in acid strength differences but instead spurious interactions in periodic DFT methods. These findings are consistent with the similar ⟨DPE⟩ values in MFI, BEA, MOR, FER, CHA, and FAU, and with the expectation that these zeolites, similar in their composition and structural building blocks, would also show similar ⟨DPE⟩ values.

The correlation shown in Figure 5, along with DPE values reported for large clusters[3] and embedded clusters[21] at isolated protons for a given location and framework, can be used to remove the spurious interactions of DFT from ⟨DPE⟩ values. Here, we use the value of 1200 kJ mol^{-1} for the DPE value of protons at the Al7−O17−Si4 site of MFI from QM-Pot[21] to adjust the periodic DFT calculation at the Al7−O17−Si4 site of 1668 kJ mol^{-1}. Figure 5 was then used to remove the spurious interactions in periodic DFT due to framework density differences to give ⟨DPE⟩ values free from the artifacts of periodic DFT methods (Figure 6). The corrected ⟨DPE⟩ values

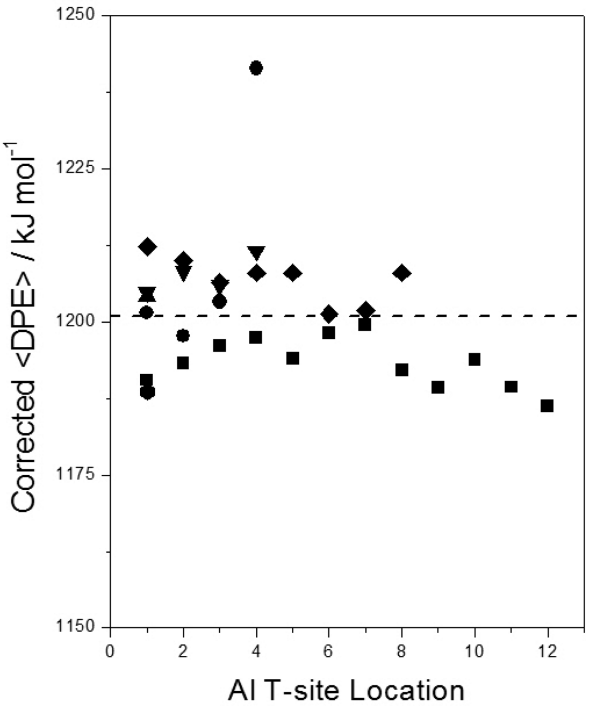

Figure 6. ⟨DPE⟩ values of zeolites calculated with eqs 3 and 4 from DFT (RPBE/PAW) on MFI (squares), BEA (diamonds), FAU (triangles), CHA (hexagon), FER (upside-down triangle), and MOR (circles) as a function of Al T-site location and corrected for spurious charge effects in periodic DFT calculations. The dotted line represents the arithmetic mean of the ⟨DPE⟩ values for all zeolites.

obtained using this protocol (Figure 6) are similar (1201 ± 11 kJ mol^{-1}; MFI, BEA, FER, MOR, CHA, FAU) on all zeolite frameworks, indicative of similar strengths for Brønsted acid sites at all locations and for all framework structures. This conclusion applies to different T-sites (section 3.1) within a given framework (in spite of their different local structure) without the need for any corrections. It is neither surprising nor suspicious that these similar acid sites are preserved, therefore, among other frameworks and their T-sites.

The ⟨DPE⟩ value for the Al4 site in MOR is noticeably larger than the ⟨DPE⟩ values at other Al and frameworks; this site resides at the mouth of the 8-MR side pockets in MOR and contains three crystallographically distinct O atoms (O10, O9, and O7 with 2-fold degeneracy), and its deprotonated form is less stable (by ∼40 kJ mol^{-1}) than the other three Al sites in MOR. The unstable nature of this anionic structure is not caused by its location at a four-ring (the "ring" nomenclature denotes the smallest number of T-sites connected through bonds with O that form a circle) and two five-ring structures, because the Al3 anion, which shares the same ring structures, is more stable by 44 kJ mol^{-1}. The instability of this Al site may reflect a combination of local structural features that lead to Al anions that are uniquely destabilized.

The ubiquitous previous claims for the different acid strength for protons associated with Al sites at different locations or zeolite frameworks[4,48−50] are not consistent with the ⟨DPE⟩ values reported here for (isolated) Al atoms present in very diverse zeolite structures (1201 ± 11 kJ mol^{-1}; MFI, BEA, FER, MOR, CHA, FAU; Figure 6). The adsorption enthalpies of probe molecules and the rates of specific catalytic reactions have often been used to support these claims for diverse acid strengths among zeolites.[1] In the next section, we examine NH_3 adsorption energies at different proton locations and zeolite frameworks in order to probe how these thermodynamic properties depend on ⟨DPE⟩ values. In a later section, we examine how reactions, through the stability of the ion-pair transition states that mediate them, sense acid strength.

3.4. NH_3 Adsorption Enthalpies at Brønsted Acid Sites and Connections to Acid Strength. NH_3 adsorption enthalpies, measured calorimetrically or less directly from NH_3 desorption rates during temperature ramping, are often used to probe acid strength because of their convenience and their sporadic and often anecdotal correlation with the rates of some acid-catalyzed reactions.[4,49,51] Here, NH_3 adsorption enthalpies were calculated at each proton location accessible to NH_3 in MFI using periodic DFT methods with PBE-D2/PAW functionals that account for van der Waals interactions (through a semiempirical dispersion additive potential).[37] Adsorption energies were corrected for zero-point vibrational energies and temperature using calculated vibrational frequencies to obtain adsorption enthalpies at 480 K (section 2.2) in order to compare with calorimetric NH_3 adsorption measurements.

Calculated adsorption enthalpies varied by 35 kJ mol^{-1} (from −119 to −154 kJ mol^{-1}) among 13 of the 16 configurations accessible to NH_3 (accessibility determined as described in section 2.2) in MFI (Figure 7), but did not trend monotonically with the DFT-derived ⟨DPE⟩ values using the RPBE/PAW functionals at each location. NH_4^+ cations formed from protons at the Al2−O13, Al3−O3, and Al4−O16 configurations led to adsorption enthalpies of −93, −80, and 2.5 kJ mol^{-1}, respectively. These adsorption enthalpies are too large to overcome entropy losses of adsorption and led to adsorption free energies that disfavor the binding of NH_4^+ at these locations at 480 K (−11.4, +1.0, and +81.0 kJ mol^{-1}).

The prevalence of H-bonding and dispersive interactions between NH_4^+ cations and the zeolite framework that do not depend on acid strength undermine any connections between adsorption enthalpies and acid strength. These interactions unrelated to those associated with acid strength and instead

DOI: 10.1021/acscatal.5b01133
ACS Catal. 2015, 5, 5741−5755

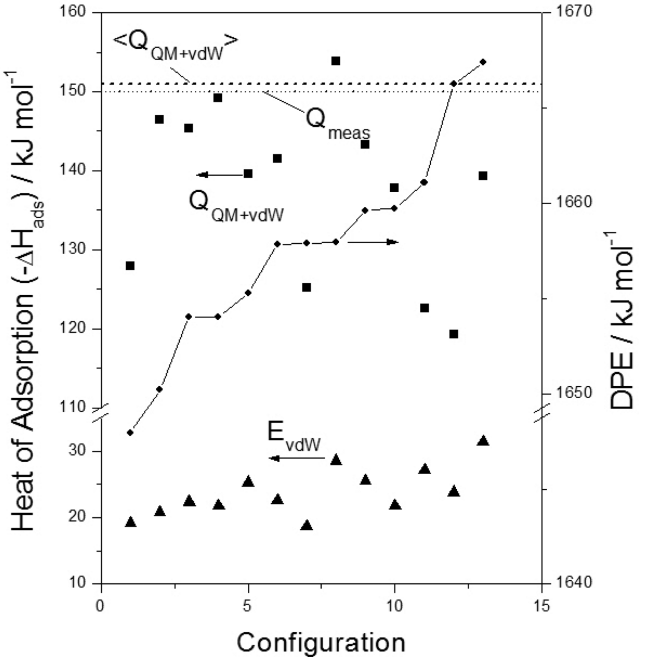

Figure 7. NH_3 adsorption enthalpies (squares; Q_{QM+vdW}; PBE-D2/PAW), NH_4^+ van der Waals interaction energies (triangles; E_{vdW}; extricated from PBE-D2/PAW energies), and DPE (circle; RPBE/PAW) calculated using DFT methods on H-MFI as functions of the Al/H^+ configuration of initial adsorption structures (in ascending DPE). Two horizontal dashed and dotted lines reflect the measured (Q_{meas}) NH_3 adsorption enthalpy in MFI (microcalorimetry, 480 K; 150 kJ mol^{-1})[52] and the ensemble-averaged ($\langle Q_{QM+vdW} \rangle$; eq 3; 480 K; 151 kJ mol^{-1}) adsorption enthalpy calculated using DFT enthalpies and free energies at 480 K assuming random siting of Al atoms within the MFI framework.

mediated by dispersion or van der Waals forces depend sensitively on the location and orientation of the NH_4^+ moieties in zeolite voids; in all cases observed here, the proton is fully transferred to NH_3 to form NH_4^+ species exhibiting two or more H-bonds with framework O atoms. The stabilization provided by H-bonding between NH_4^+ species and framework O atoms depends on the angles and distances in the N−H−O structures that form much more strongly than the small and tightly held proton that was transferred; such H-bonding interactions may contribute as much as 60 kJ mol^{-1} for each N−H−O bond (estimated from MP2 calculations of NH_3 binding to zeolite clusters)[53] to adsorption enthalpies. Furthermore, van der Waals interactions account for >12% of the adsorption energies at all proton locations in MFI (Figure 7); these dispersion components were estimated from the van der Waals portion of the energies extracted from the semiempirical corrections to the PBE-D2 functionals.[37] The lack of discernible trends between NH_3 adsorption enthalpies and ⟨DPE⟩ values (Figure 7), and the predominant role of H-bonding and van der Waals forces in determining the magnitude of the NH_3 adsorption enthalpies provide compelling evidence that such enthalpies reflect, to a predominant extent, interactions that are essentially insensitive and indirectly influenced, if at all, by acid strength.

Such insensitivity of NH_3 adsorption enthalpies to acid strength may seem surprising at first glance because of the ion-pair nature of the NH_4^+−zeolite interaction and the expected effect of the stability of the conjugate anion on the propensity for proton transfer.[12] Yet, the influence of DPE on ion-pair formation energies, such as those for CH_3OH dehydration transition states,[54] is attenuated because the resulting ionic interactions recover a large portion of the energy required for deprotonating the acid. This attenuation explains, in part, the negligible influence of DPE on NH_3 adsorption enthalpies. In fact, the independent effects of confinement (dispersion and H-bonding interactions) also contribute to the confusing indirect consequences of proton location on NH_3 adsorption enthalpies in microporous aluminosilicates.

The use of the thermodynamics (or the dynamics) of NH_3 adsorption−desorption processes as a descriptor of acid strength cannot be supported by theoretical assessments or by any conceptual framework appropriate to rigorously describe the proton-donating tendencies of acids. We surmise that even in the case of solid acids with less confining porous structures, the specific geometry at the acid site will influence the extent of H-bonding and thus the adsorption enthalpies to an extent that would make NH_3 adsorption enthalpies an inappropriate indicator of acid strength. Even in such cases, small cationic species, such as NH_4^+, will recover most of the ionic and covalent interactions lost upon deprotonation of the acid via interactions with the conjugate anion,[55] thus significantly attenuating the effects of DPE on adsorption enthalpies.

On MFI, measured NH_3 adsorption enthalpies (microcalorimetry; Si/Al ratios of 35 and 70; 150 kJ mol^{-1}; 480 K)[52] lie within the range of our theoretical estimates (119−154 kJ mol^{-1}; Figure 7), indicating that the DFT models and functionals used here describe the relevant energetics. Measured NH_3 adsorption enthalpies, which represent ensemble averages over all Al and proton locations, are not directly comparable with individual NH_3 adsorption enthalpies at each T-site proton because the latter do not reflect the thermodynamic sampling of the Al and proton locations in measured samples. Instead, the thermodynamic distribution of NH_4^+ and their enthalpies over all accessible and realistic (i.e., the crystallographic Al atom exists in the measured sample) locations must be considered and appropriately ensemble-averaged to compare with measured adsorption enthalpies. This comparison is rigorous when the locations and distributions of Al are known; Al locations, however, are rarely accessible to experimentation.[13] For the specific case of random Al siting, the ensemble-averaged NH_3 adsorption enthalpy can be calculated from the enthalpies and free energies of each NH_4^+ state at each Al site (16 accessible) with eq 3 (with enthalpies instead of energies); this ensemble-averaged NH_3 adsorption enthalpy is 151 kJ mol^{-1} at 480 K (Figure 7), in excellent agreement with measured enthalpies of 150 kJ mol^{-1} at 480 K.[52]

These conclusions demonstrate that the occasional correlations between NH_3 adsorption enthalpies and activation energies for some catalytic reactions do not reflect changes in acid strength except for some special cases. These special cases involve changes in acid strength (DPE) that do not result in appreciable changes in the H-bonding and dispersive interactions of NH_4^+ species, such as the increase in propene methylation turnover rates with NH_3 adsorption enthalpies on a series of CHA-type frameworks with different compositions (and thus acid strength) and a single crystallographically unique T-site (and thus similar confinement of NH_4^+).[51] These correlations cannot be taken as justifications of a general approach unsupported by theory and by the concept of acid strength because of their reliance on specific and intermittent changes in acid strength and not structure. Many more

DOI: 10.1021/acscatal.5b01133
ACS Catal. 2015, 5, 5741−5755

Scheme 2. Thermochemical Cycle of an Acid Catalyzed Activation of R in a Zeolite Depicting the Energy Levels of Various Equilibrated Protons (ZH) and Transition States (TS) and Their Averages (⟨ZH⟩ and ⟨TS⟩) Reflected in Activation Barriers $\langle E_a^{\ddagger} \rangle$ and Their Relationship with Deprotonation Energies (DPE), Proton Affinities (E_{PA}), and Interaction Energies ($\langle E_{inter} \rangle$)

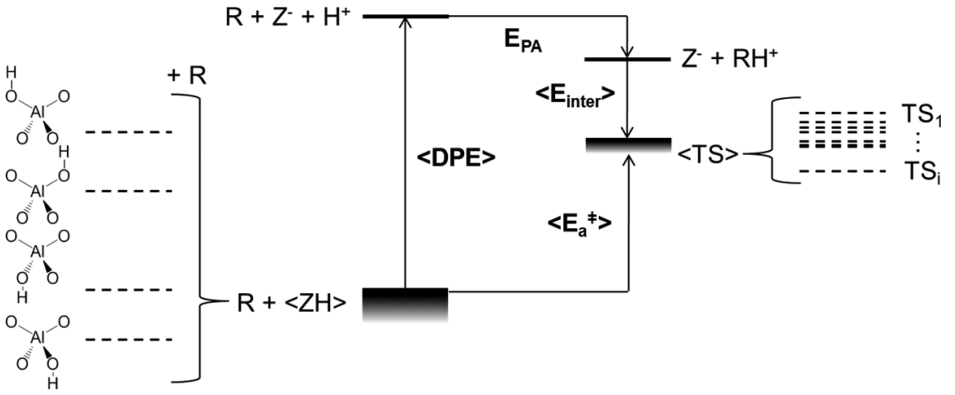

counterexamples exist, such as the lack of correlations of NH_3 adsorption enthalpies with CH_3OH dehydration[3] or hexane cracking[7] rate constants on MFI with Al, Ga, Fe, or B heteroatoms in spite of the >10 kJ mol^{-1} DPE differences and similar structure of these samples.[3]

We find that measured NH_3 adsorption enthalpies do not reflect acid strength differences, but instead reflect a thermodynamic distribution of NH_4^+ moieties interacting with the zeolite and conjugate anion at different locations, with enthalpies that depend on the shape and size of the pore. Measured turnover rates, by analogy, also depend on the distributions of transition states and reactive intermediates at acid sites. As a result, the occasional correlations reported for adsorption enthalpies with turnover rates must be treated as coincidences, made possible by situations in which the confinement effects and ionic stabilization of NH_3 (or of any other adsorbed probe molecule) and of the relevant transition states (relative to their reactive precursors) fortuitously correlate. In the next section, transition state theory formalisms and thermodynamic treatments of equilibrated states are exploited to understand the connections between DPE and reactivity.

3.5. Relations between Acid Strength and Reactivity Using the Formalism of Transition State Theory. The reactivity of Brønsted acids and its practical manifestation as turnover rates depend on DPE values because the latter accounts for the energy required to transfer a proton to a precursor species to form the ion-pair transition states that mediate acid-catalyzed reactions (Scheme 2).[12] Weaker acids, with their larger DPE values, require larger energies to detach the proton; the transition states at weaker acids, with their more diffuse charge and larger distances from the conjugate anion than the proton, recover only part of the ionic interactions of the starting proton with the same anion, thus leading to larger activation barriers.[54] Measured activation barriers and reaction rates invariably reflect a distribution of transition states and reactive intermediates at all accessible protons in zeolites. Any attempt to relate measured turnover rates with the discrete DPE values at each T-site requires statistical averages of DPE values (to ⟨DPE⟩) among all T-sites, and an understanding of the connections between ⟨DPE⟩ and the statistical representations of rates.

The distribution of protons among the four O atoms at each T-site that contains an Al atom (Scheme 1) leads to a calculable expected ⟨DPE⟩ value at each T-site location (Figure 1). This value is related to the distribution of transition states (equilibrated with reactive intermediates) at the same Al T-site using a thermochemical cycle, depicted in Scheme 2 and conveniently chosen. In such hypothetical cycles, made possible by the state function nature of enthalpies and free energies, a proton pool (⟨ZH⟩) equilibrated among all locations at a T-site is first deprotonated at an energy cost given by ⟨DPE⟩ to form the conjugate anion and a gaseous H^+. Next, a gaseous reactant (R) is protonated by this gaseous H^+ to form a gaseous analog of the relevant transition state (RH^+). The RH^+ moiety is then allowed to interact with the conjugate anion and with the surrounding framework to form the pool of transition states (⟨TS⟩), equilibrated among all locations at a T-site. The ensemble-averaged activation barrier relative to gaseous reactants ($\langle E_a^{\ddagger} \rangle$) is then related to ⟨DPE⟩ by the proton affinity of the reactant (E_{PA}) and the average interaction energy of the gaseous transition state with the zeolite framework ($\langle E_{inter} \rangle$)

$$\langle E_a^{\ddagger} \rangle = \langle \mathrm{DPE} \rangle + E_{PA} + \langle E_{inter} \rangle \quad (6)$$

Equation 6 applies when the activation barrier reflects the difference in energy between the transition state and gaseous reactants (and ⟨ZH⟩). These treatments can be expanded to include the more general case of activation barriers relative to neutral or charged intermediates by the subtraction of their respective ensemble-averaged adsorption energies (e.g., $\langle E_{ads} \rangle$) from the right side of eq 6; these intermediate species may or may not differ in size and charge from the transition state, and thus have different components of ionic, covalent, and van der Waals stabilization, and will be affected by acid strength differences to a lesser extent than transition states. The average activation barrier relative to gaseous reactants is determined by the statistical distribution of protons and transition states and their interaction energies at a given Al site, and is equivalent to the measured activation barrier for a given temperature when these barriers reflect the energies of transition states with respect to gaseous reactants (or intermediates with the subtraction of $\langle E_{ads} \rangle$).

Equation 6 and Scheme 2 demonstrate that activation energies, and thus also turnover rates, depend on the distribution of transition states and protons among T-sites. Theoretical comparisons with measured kinetic and thermodynamic values must reflect these distributions as shown by the large variance in NH_3 adsorption enthalpies at discrete locations (section 3.4). As an approximation and in lieu of

DOI: 10.1021/acscatal.5b01133
ACS Catal. 2015, 5, 5741−5755

calculating all possible states using DFT, a subset of the most thermodynamically stable protons, transition states, and intermediates could be used to compare with real samples, because the most stable states disproportionately contribute to ensemble-averaged energy values. The most stable proton configurations, their optimized structures (RPBE/PAW), and their energies are given in this work for reference in the Supporting Information.

The calculated distribution of transition states and protons at a T-site can be related to activation barriers using the following framework developed from statistical mechanics and transition state theory (TST). The turnover rate of a catalytic reaction at an Al site (r_{Al}) is given by additive terms in which transmission frequencies, υ_i, are multiplied by the concentration of each transition state

$$r_{Al} = \sum_{i=1}^{N} r_i = \sum_{i=1}^{N} \upsilon_i[TS_i] \tag{7}$$

The quasi-equilibrium of transition states with precursors (discussed here for the case of gaseous reactants) in TST then gives

$$r_{Al} = \frac{k_B T}{h} \sum_{i=1}^{N} e^{-\Delta G_i^{\ddagger}/k_B T} \prod_j a_j^{\nu_j} \tag{8}$$

which relates the overall rate to the activation free energies ($\Delta G_i^{\ddagger}$) required to form transition states from gaseous reactants present at a thermodynamic activity, a_j, and reaction stoichiometry, ν_j. The overall measured reaction rate reflects an average activation free energy ($\langle \Delta G^{\ddagger} \rangle$) relative to gaseous reactants and the thermodynamic distribution of protons (<ZH>; each discrete activation free energy ($\Delta G_i^{\ddagger}$) must also be referenced to the same arbitrary reference state)

$$r_{Al} = \frac{k_B T}{h} e^{-\langle \Delta G^{\ddagger} \rangle / k_B T} \prod_j a_j^{\nu_j} \tag{9}$$

Combining eqs 8 and 9 and canceling activity terms because they correspond to the same gaseous reactants gives

$$e^{-\langle \Delta G^{\ddagger} \rangle / k_B T} = \sum_{i=1}^{N} e^{-\Delta G_i^{\ddagger}/k_B T} \tag{10}$$

Equation 10 gives the measured free energy activation barrier ($\langle \Delta G^{\ddagger} \rangle$; averaged over all transition states at a T-site) in terms of the barriers to form each transition state from gaseous reactants and the equilibrium distribution of protons ($\langle$ZH$\rangle$ in Scheme 2). The measured (averaged) activation enthalpy can be obtained from these (averaged) free energies of activation using the van't Hoff relationship:

$$\frac{\partial \ln(\langle K^{\ddagger} \rangle)}{\partial \frac{1}{T}} = \frac{\partial \langle \Delta G^{\ddagger} \rangle}{\partial \frac{1}{T}} = -\frac{\langle \Delta H^{\ddagger} \rangle}{k_B} \tag{11}$$

Combining eqs 10 and 11 gives the averaged activation enthalpy as

$$\langle \Delta H^{\ddagger} \rangle = \frac{\sum_{i=1}^{N} \left[\Delta H_i^{\ddagger} \exp\left(\frac{-\Delta G_i^{\ddagger}}{k_B T} \right) \right]}{\sum_{i=1}^{N} \exp\left(\frac{-\Delta G_i^{\ddagger}}{k_B T} \right)} \tag{12}$$

Here, the average activation enthalpy ($\langle \Delta H^{\ddagger} \rangle$) reflects the enthalpy required to form transition states equilibrated at a T-site ($\langle$TS$\rangle$ in Scheme 2) from gaseous reactants and protons equilibrated at each T-site ($\langle$ZH$\rangle$ in Scheme 2). Equation 12 is equivalent to the Boltzmann-type average used to estimate $\langle$DPE$\rangle$ values, eq 3, when enthalpies are replaced by energies. Equation 12 can be simply extended to include multiple isolated T-site locations and densities by adding a second summation through all T-sites to the numerator and denominator; this is derived from the analogous second summation added to the right side of eq 10.

These treatments indicate that activation enthalpies reflect an ensemble-averaged distribution of transition state energies at a T-site. Larger $\langle$DPE$\rangle$ values reflect weaker acids and result in larger activation barriers because the stability of the conjugate anion uniquely determines the ionic stability of the ensemble of protons, transition states, and reactive species (Scheme 2). The statistical treatments of protons are a thermodynamic extension to the discrete calculations of DFT and are particularly necessary for acids with the equilibrated distribution of states. For zeolites, the distributions of protons at each Al T-site result in $\langle$DPE$\rangle$ values that erase the differences found in DPE values.

The similar values of the corrected $\langle$DPE$\rangle$ for MFI, BEA, MOR, FER, FAU, and CHA zeolites (1201 ± 11 kJ mol^{-1}; Figure 6) and Scheme 2 indicate that these zeolites stabilize transition states and their reactive intermediates with ionic interactions to similar extents because $\langle$DPE$\rangle$ values reflect the ability of the conjugate anion to stabilize charge. Therefore, we expect that reaction rates of zeolites will depend only on the dispersive and H-bonding interaction differences of their transition states (relative to reactive intermediates) because the ionic interactions of the acid sites with transition states would be similar at each Al. This conclusion is consistent with methanol dehydration rate constants, which reflect the energy of dimethyl ether formation transition states to H-bonded methanol, that increase systematically with the tighter confinement of transition states on a wide range of zeolite frameworks (FAU, SFH, BEA, MOR, MTW, MFI, MTT), because in these reactions transition states are larger than H-bonded methanol and in turn are stabilized more by confinement differences.[5] Also, the similar strength of zeolite acids given by $\langle$DPE$\rangle$ is consistent with the similar intrinsic activation barriers for monomolecular propane cracking (199 ± 11 kJ mol^{-1}, on FAU, BEA, MOR, MFI, MWW, and FER)[11,56] and dehydrogenation (237 ± 8 kJ mol^{-1}, on MFI, FER, and MOR)[15] on several zeolite frameworks, which both reflect enthalpy differences of confined transition states and adsorbed alkoxide reactants that are similar in size and thus stabilized to similar extents by confinement.[12,54] These results suggest that reactivity differences between zeolite frameworks can be predicted with force-fields that reflect the dispersive and H-bonding interactions of transition states at relevant locations in different frameworks.

The relevance of $\langle$DPE$\rangle$ values to transition state energy distributions reflected in catalytic rates suggests that $\langle$DPE$\rangle$ values are more appropriately suited for describing acid strength differences that matter for catalysis than DPE. For samples with similar composition, such as zeolites, $\langle$DPE$\rangle$ values erase the discrepancies in DPE values and show that the catalytically relevant strength of the acid depends only on the composition of the T-site (Si−O(H)−Al) and thus its ability to stabilize charge.

DOI: 10.1021/acscatal.5b01133
ACS Catal. 2015, 5, 5741−5755

4. CONCLUSIONS

The characterization of Brønsted acid strength, rigorously defined as the energy required to separate the conjugate base from the proton (DPE), is fundamental to the understanding of acid catalysis and the comparison of Brønsted acids for reactivity and selectivity. Experimental probes of acid strength in zeolites and solid acids in general, such as adsorption enthalpies of molecules or catalytic turnover rates, invariably reflect dispersive or van der Waals interactions of the probe that do not reflect the strength of the acid site.

DPE values of several aluminosilicates (MFI, BEA, MOR, FER, FAU, and CHA) depend sensitively (by 77 kJ mol^{-1}) on the location of Al and protons at crystallographically unique positions. The statistical ensemble averages of these DPEs (⟨DPE⟩) at each crystallographically unique Al position, however, erase the differences in DPE because they reflect a similar stability of the conjugate anion regardless of Al location or framework structure. We find that the isolating nature of the zeolite framework and the mobility of protons in the presence of catalytic amounts of water lead to an acid strength that depends only on the identity of the heteroatom species (e.g., Al) and not on its location, distribution, or density.

NH_3 adsorption, and by inference the adsorption of other molecules, depends sensitively on interactions (H-bonding and dispersive) that do not reflect, and are often independent of, acid strength. These interactions and the attenuation of the effects of acid strength on adsorption enthalpies result in NH_3 adsorption enthalpies that do not correlate with any measure of acid strength (DPE or ⟨DPE⟩). DPE values also do not correlate with the vibrational frequency or length of O−H bonds, or with Si−O−Al bond angles. The use of NH_3 adsorption−desorption processes or structural features as descriptors of acid strength cannot be supported by these theoretical assessments.

The reactivity of zeolites, and solid acids in general, depend on the stability of the distribution of transition states relative to the distribution of reactive intermediates or protons. The ensemble-averaged transition state energy reflects, in part, the ensemble-averaged DPE (⟨DPE⟩) because of the analogous electrostatic interactions present at ion-pair transition states and protons. MFI, BEA, MOR, FER, FAU, and CHA share similar ⟨DPE⟩ values, and therefore stabilize transition states with electrostatic interactions to similar extents. We conclude that turnover rate differences reflect instead the diversity of zeolite void shapes and sizes that confine transition states and reactive intermediates to different extents. This work demonstrates the necessity of statistical treatments of DFT-derived energies, enthalpies, and free energies for their comparison with measured values, which unavoidably involve the thermodynamic distributions of reactive species. In the case of zeolites, ensemble averages erase the subtle differences in acid strength at different Al and H^+ configurations and demonstrate the remarkably similar catalytically relevant acid strength of zeolites.

■ ASSOCIATED CONTENT

Supporting Information

The Supporting Information is available free of charge on the ACS Publications website at DOI: 10.1021/acscatal.5b01133.

Optimized structures and energies (RPBE/PAW) of the most stable proton configurations (ZIP)

Figures showing the relationships between ν(OH) frequencies, O−H bond distances, DPE, and Si−O−Al bond angles in MFI (PDF)

■ AUTHOR INFORMATION

Corresponding Authors

*Fax: + 1 (510) 642-4778. E-mail: a.jones@berkeley.edu.
*Fax: + 1 (510) 642-4778. E-mail: iglesia@berkeley.edu.

Notes

The authors declare no competing financial interest.

■ ACKNOWLEDGMENTS

The authors thank Dr. Prashant Deshlahra (UC Berkeley), Dr. David Hibbitts (UC Berkeley), and Will Knaeble (UC Berkeley) for useful discussions. We also thank Prof. Joachim Sauer (Humboldt University) and Dr. Marcin Rybicki (Humboldt University) for technical discussions about the artifacts in periodic calculations and their comparison with QM-Pot methods. We gratefully acknowledge the financial support for this research from the Chevron Energy Technology Company and supercomputing resources provided by the XSEDE Science Gateways program (CHE140066).

■ REFERENCES

(1) Corma, A. *Chem. Rev.* **1995**, *95*, 559−614.
(2) Gorte, R. J. *Catal. Lett.* **1999**, *62*, 1−13.
(3) Jones, A. J.; Carr, R. T.; Zones, S. I.; Iglesia, E. *J. Catal.* **2014**, *312*, 58−68.
(4) Farneth, W. E.; Gorte, R. J. *Chem. Rev.* **1995**, *95*, 615−635.
(5) Jones, A. J.; Zones, S. I.; Iglesia, E. *J. Phys. Chem. C* **2014**, *118*, 17787−17800.
(6) Boronat, M.; Corma, A. *Catal. Lett.* **2015**, *145*, 162−172.
(7) Parrillo, D. J.; Lee, C.; Gorte, R. J.; White, D.; Farneth, W. E. *J. Phys. Chem.* **1995**, *99*, 8745−8749.
(8) Derouane, E. G. *Microporous Mesoporous Mater.* **2007**, *104*, 46−51.
(9) Derouane, E. G. *J. Catal.* **1986**, *100*, 541−544.
(10) De Moor, B. A.; Reyniers, M. F.; Gobin, O. C.; Lercher, J. A.; Marin, G. B. *J. Phys. Chem. C* **2011**, *115*, 1204−1219.
(11) Gounder, R.; Iglesia, E. *Chem. Commun.* **2013**, *49*, 3491−3509.
(12) Rigby, A. M.; Kramer, G. J.; vanSanten, R. A. *J. Catal.* **1997**, *170*, 1−10.
(13) Dědeček, J.; Sobalík, Z.; Wichterlová, B. *Catal. Rev.: Sci. Eng.* **2012**, *54*, 135−223.
(14) Sklenak, S.; Dedecek, J.; Li, C.; Wichterlova, B.; Gabova, V.; Sierka, M.; Sauer, J. *Phys. Chem. Chem. Phys.* **2009**, *11*, 1237−1247.
(15) Gounder, R.; Iglesia, E. *J. Am. Chem. Soc.* **2009**, *131*, 1958−1971.
(16) Sastre, G.; Fornes, V.; Corma, A. *J. Phys. Chem. B* **2002**, *106*, 701−708.
(17) Brand, H. V.; Curtiss, L. A.; Iton, L. E. *J. Phys. Chem.* **1993**, *97*, 12773−12782.
(18) Brand, H. V.; Curtiss, L. A.; Iton, L. E. *J. Phys. Chem.* **1992**, *96*, 7725−7732.
(19) Yuan, S. P.; Wang, J. G.; Li, Y. W.; Jiao, H. *J. Phys. Chem. A* **2002**, *106*, 8167−8172.
(20) Chatterjee, A.; Iwasaki, T.; Ebina, T.; Miyamoto, A. *Microporous Mesoporous Mater.* **1998**, *21*, 421−428.
(21) Brandle, M.; Sauer, J. *J. Am. Chem. Soc.* **1998**, *120*, 1556−1570.
(22) Lo, C.; Trout, B. L. *J. Catal.* **2004**, *227*, 77−89.
(23) Grajciar, L.; Arean, C. O.; Pulido, A.; Nachtigall, P. *Phys. Chem. Chem. Phys.* **2010**, *12*, 1497−1506.
(24) Kresse, G.; Hafner, J. *Phys. Rev. B: Condens. Matter Mater. Phys.* **1993**, *47*, 558−561.
(25) Kresse, G.; Furthmüller, J. *Comput. Mater. Sci.* **1996**, *6*, 15−50.

DOI: 10.1021/acscatal.5b01133
ACS Catal. 2015, 5, 5741−5755

(26) Kresse, G.; Furthmüller, J. *Phys. Rev. B: Condens. Matter Mater. Phys.* **1996**, *54*, 11169−11186.
(27) Kresse, G.; Hafner, J. *Phys. Rev. B: Condens. Matter Mater. Phys.* **1994**, *49*, 14251−14269.
(28) Hammer, B.; Hansen, L. B.; Nørskov, J. K. *Phys. Rev. B: Condens. Matter Mater. Phys.* **1999**, *59*, 7413−7421.
(29) Blöchl, P. E. *Phys. Rev. B: Condens. Matter Mater. Phys.* **1994**, *50*, 17953−17979.
(30) Kresse, G.; Joubert, D. *Phys. Rev. B: Condens. Matter Mater. Phys.* **1999**, *59*, 1758−1775.
(31) McQuarrie, D. A. *Statistical Mechanics*; University Science Books: Sausolito, 2000.
(32) Baerlocher, C.; McCusker, L. B. Database of Zeolite Structures. http://www.iza-structure.org/databases/ (accessed January 8, 2014).
(33) Van Koningsveld, H.; Van Bekkum, H.; Jansen, J. C. *Acta Crystallogr., Sect. B: Struct. Sci.* **1987**, *43*, 127−132.
(34) Olson, D. H.; Kokotailo, G. T.; Lawton, S. L.; Meier, W. M. *J. Phys. Chem.* **1981**, *85*, 2238−2243.
(35) Freysoldt, C.; Neugebauer, J.; Van de Walle, C. G. *Phys. Rev. Lett.* **2009**, *102*, 016402.
(36) Bruneval, F.; Crocombette, J.-P.; Gonze, X.; Dorado, B.; Torrent, M.; Jollet, F. *Phys. Rev. B: Condens. Matter Mater. Phys.* **2014**, *89*, 045116.
(37) Grimme, S. *J. Comput. Chem.* **2006**, *27*, 1787−1799.
(38) Haranczyk, M. Zeo++. http://www.carboncapturematerials.org/Zeo++.
(39) Willems, T. F.; Rycroft, C. H.; Kazi, M.; Meza, J. C.; Haranczyk, M. *Microporous Mesoporous Mater.* **2012**, *149*, 134−141.
(40) Gounder, R.; Jones, A. J.; Carr, R. T.; Iglesia, E. *J. Catal.* **2012**, *286*, 214−223.
(41) Ryder, J. A.; Chakraborty, A. K.; Bell, A. T. *J. Phys. Chem. B* **2000**, *104*, 6998−7011.
(42) Freysoldt, C.; Neugebauer, J.; Van de Walle, C. G. *Phys. Status Solidi B* **2011**, *248*, 1067−1076.
(43) Eichler, U.; Brandle, M.; Sauer, J. *J. Phys. Chem. B* **1997**, *101*, 10035−10050.
(44) Cioslowski, J.; Liu, G. H.; Castro, R. A. M. *Chem. Phys. Lett.* **2000**, *331*, 497−501.
(45) Peng, L.; Huo, H.; Liu, Y.; Grey, C. P. *J. Am. Chem. Soc.* **2007**, *129*, 335−346.
(46) Huo, H.; Peng, L.; Grey, C. P. *J. Phys. Chem. C* **2011**, *115*, 2030−2037.
(47) Jones, A. J.; Iglesia, E. *Angew. Chem., Int. Ed.* **2014**, *53*, 12177−12181.
(48) Corma, A. *Curr. Opin. Solid State Mater. Sci.* **1997**, *2*, 63−75.
(49) Lercher, J. A.; Grundling, C.; EderMirth, G. *Catal. Today* **1996**, *27*, 353−376.
(50) Kramer, G. J.; Van Santen, R. A. *J. Am. Chem. Soc.* **1993**, *115*, 2887−2897.
(51) Wang, C.-M.; Brogaard, R. Y.; Weckhuysen, B. M.; Nørskov, J. K.; Studt, F. *J. Phys. Chem. Lett.* **2014**, *5*, 1516−1521.
(52) Parrillo, D. J.; Gorte, R. J. *J. Phys. Chem.* **1993**, *97*, 8786−8792.
(53) Teunissen, E. H.; Van Duijneveldt, F. B.; Van Santen, R. A. *J. Phys. Chem.* **1992**, *96*, 366−371.
(54) Carr, R. T.; Neurock, M.; Iglesia, E. *J. Catal.* **2011**, *278*, 78−93.
(55) Deshlahra, P.; Carr, R. T.; Iglesia, E. *J. Am. Chem. Soc.* **2014**, *136*, 15229−15247.
(56) Xu, B.; Sievers, C.; Hong, S. B.; Prins, R.; van Bokhoven, J. A. *J. Catal.* **2006**, *244*, 163−168.

DOI: 10.1021/acscatal.5b01133
ACS Catal. 2015, 5, 5741−5755